Acta Biomaterialia 138 (2022) 112–123

Contents lists available at ScienceDirect

Acta Biomaterialia

journal homepage: www.elsevier.com/locate/actbio

Full length article

Magnetic nanocomposite hydrogel with tunable stiffness for probing cellular responses to matrix stiffening

Tianhao Yan, Depeng Rao, Ye Chen, Yu Wang, Qingchuan Zhang*, Shangquan Wu*

CAS Key Laboratory of Mechanical Behavior and Design of Material, Department of Modern Mechanics, University of Science and Technology of China, Hefei 230027, China

ARTICLE INFO

Article history:
Received 19 July 2021
Revised 8 October 2021
Accepted 1 November 2021
Available online 6 November 2021

Keywords:
Magnetic nanocomposite hydrogel
Fe_3O_4 magnetic nanoparticles
Matrix stiffening
Human mesenchymal stem cells
Morphology

ABSTRACT

As cells have the capacity to respond to their mechanical environment, cellular biological behaviors can be regulated by the stiffness of extracellular matrix. Moreover, biological processes are dynamic and accompanied by matrix stiffening. Herein, we developed a stiffening cell culture platform based on polyacrylamide-Fe_3O_4 magnetic nanocomposite hydrogel with tunable stiffness under the application of magnetic field. This platform provided a wide range of tunable stiffness (~0.3–20 kPa) covering most of human tissue elasticity with a high biocompatibility. Overall, the increased magnetic interactions between magnetic nanoparticles reduced the pore size of the hydrogel and enhanced the hydrogel stiffness, thereby facilitating the adhesion and spreading of stem cells, which was attributed to the F-actin assembly and vinculin recruitment. Such stiffening cell culture platform provides dynamic mechanical environments for probing the cellular response to matrix stiffening, and benefits studies of dynamic biological processes.

Statement of significance

Cellular biological behaviors can be regulated by the stiffness of extracellular matrix. Moreover, biological processes are dynamic and accompanied by matrix stiffening. Herein, we developed a stiffening cell culture platform based on polyacrylamide/Fe_3O_4 magnetic nanocomposite hydrogels with a wide tunable range of stiffness under the application of magnetic field, without adversely affecting cellular behaviors. Such matrix stiffening caused by enhanced magnetic interaction between magnetic nanoparticles under the application of the magnetic field could induce the morphological variations of stem cells cultured on the hydrogels. Overall, our stiffening cell culture platform can be used not only to probe the cellular response to matrix stiffening but also to benefit various biomedical studies.

1. Introduction

Cellular biological behaviors are not only regulated by intracellular factors, but also closely related to the mechanical properties of extracellular matrix (ECM) [1]. As one of the most important mechanical properties, the stiffness of the ECM can greatly affect the biological behaviors of cell, such as spreading, morphology, migration, proliferation, and differentiation [1–6]. For instance, when the ECM stiffness is similar to the elasticity of human tissue (brain: ~0.1–1 kPa; muscle: ~8–17 kPa; bone: ~25–40 kPa), stem cells will tend to differentiate into that particular tissue and display appropriate morphology of that tissue [1]. Furthermore, cells exhibited numerous morphological variations relating to difference in ECM stiffness [2]. The cells cultured on the softer substrate were less distributed with a smaller cell area. Conversely, cells cultured on the stiffer substrates spread much greater and produced more actin fibers [3,4]. While these cellular biological behaviors were always accompanied by variations in cell morphology, cell morphology could in turn impact a range of biological behaviors of cells [7–11]. Specifically, the morphology of stem cells not only significantly affected the gene expression and protein synthesis of cells [7,8], but also forecasted even influenced the lineage fates of stem cells [9–11]. The round morphology increased adipogenic differentiation whereas elongated morphology cells enhanced osteogenesis [11]. These examples demonstrated that figuring out the cellular responses to variable stiffness of ECM was key to studying the cellular biological behaviors.

Although, some significant advances have been achieved in the influence of substrate stiffness on the biological behaviors of cells,

* Corresponding authors.
E-mail addresses: zhangqc@ustc.edu.cn (Q. Zhang), wushq@ustc.edu.cn (S. Wu).

https://doi.org/10.1016/j.actbio.2021.11.001
1742-7061/

the stiffness of these substrates are almost static, lacking of dynamic characteristics. In contrast, many biological events were accompanied by matrix stiffening. For example, growing tissues increased their stiffness in response to variations in mechanical loading [12]. In addition, the fibrosis after myocardial infarction began with the deposition of massive ECM, which together with the necrotic tissue caused myocardium stiffening [13,14]. For tumor cells, the enhancement of matrix stiffness promoted tumor growth and migration [15]. These studies demonstrated that matrix stiffening was not only regarded as a disease outcome, but also as a contributing factor to disease progression. With these examples in mind, there is a great interest and desire for the substrate with dynamic stiffening to better simulate the biomechanical environment *in vivo* and investigate these processes.

To address this aspect, some hydrogel systems have been reported that can dynamically controlled their stiffness in response to external stimuli, yet only a portion of the systems were used for cell culture and thus for regulating cell behavior. For instance, temperature was used to alter hydrogel stiffness [16,17], but only with hydrophobicity changes and long reaction time. Furthermore, it was unknown whether cells could be cultured on these thermotunable hydrogels, let alone the cellular response to tunable stiffness. In addition, pH-responsive hydrogels were also applied to regulate cell behavior [18,19]. However, pH directly affected the biological behavior of cells [20], which made it difficult to distinguish the cellular response to dynamic stiffening from the response to pH variations. What's worse, their pH could damage cell viability [21]. As an alternative, dynamic phototuning hydrogels have been reported [22–26]. However, UV light damaged DNA and cell activity [27]. Moreover, calcium may alter cell signaling, and the long-term stability of the alginate composite hydrogels was limited [22]. Subsequently, Lee et al. used another photosensitive hydrogel whose stiffness could be stiffened by blue light irradiation [28]. But the blue light was a high-energy visible light which caused damage to mitochondrial DNA and cell activity [29]. Also, the tunable stiffness range of this substrate was limited (∼5–10 kPa), which was insufficient to cover most of the stiffness of human tissues (∼0.1–40 kPa). For all these reasons, a cell culture platform with high cytocompatibility and wide tunable stiffness range is urgently needed, in order to minimize any potential interference with cell behaviors and reflect actual dynamic biomechanical properties of human tissues.

In this regard, as a kind of smart biomaterials, hydrogels have been broadly applied in biomedical engineering, due to their excellent cytocompatibility, stability, and mechanical properties [30–35]. Despite the superior performances of hydrogels, a limitation of hydrogel systems is that their mechanical properties are almost invariable after preparation, lacking of active response properties [33,35]. For example, it is challenging for hydrogel tissue systems to provide dynamic biomechanical properties for simulating native tissues due to the absence of matrix stiffening [34]. Hydrogels can be integrated with magnetic nanoparticles (MNPs) to synthesize magnetic nanocomposite hydrogels which can rapidly respond to a magnetic field (MF), allowing for active response properties [35,36]. In this way, magnetic hydrogels can be tuned by external MF for their volume, configuration, structure, temperature, and magnetorheological properties to enable a wide range of biomedical applications such as tissue engineering, drug delivery and release, and cancer therapy [35–41]. However, there are few studies of magnetic nanocomposite hydrogels with tunable stiffness to investigate cellular responses (such as cell morphology) to dynamic mechanical properties (such as matrix stiffening).

Here, we developed a stiffening cell culture platform based on polyacrylamide (PAAm)-Fe_3O_4 magnetic nanocomposite hydrogels by using MF. We calculated the parameters for altering the response of the hydrogel stiffness to the MF, and then evaluated the effect of these parameters in the hydrogel response, with the goal of maximizing the tunable range of hydrogel stiffness. We subsequently obtained the mechanism of the variation of hydrogel stiffness and the relationship between pore size and stiffness by structural characterization of hydrogels. After optimizing the application method of the MF and assaying the biocompatibility of the hydrogels, the human mesenchymal stem cells (hMSCs) under different conditions were subject to quantitative morphometric analysis, thus probing cellular responses to dynamic stiffening.

2. Materials and methods

2.1. Materials

Ferric chloride hexahydrate ($FeCl_3$•$6H_2O$), sodium acetate anhydrous (CH_3COONa, NaAC), Polyacrylic acid (PAA), 3-Aminopropyltrimethoxysilane (APTES), formaldehyde, TRITON-X-100, 6-diamidino-2-phenylindole (DAPI), and TRITC-phalloidin were purchased from Sigma-Aldrich (St. Louis, MO, USA). Diethylene glycol (DEG), ethylene glycol (EG), acrylamide (AM), N, N'-Methylenebisacrylamide (BIS), ammonium persulfate (AP), N,N,N',N'-tetramethylethylenediamine (TEMED), glutaraldehyde, acetic acid, and ethanol were provided by Sinopharm Chemical Reagent Co., Ltd. (Shanghai, China). Dulbeco's modified Eagle's medium (DMEM), fetal bovine serum (FBS), penicillin-streptomycin, Phosphate-buffered saline (PBS), and trypsin-ethylenediaminetetraacetic acid (trypsin-EDTA) were sourced from Gibco (Carlsbad, CA, USA). Rat-tail tendon collagen type I was obtained from Shanghai Canspec Scientific Instruments Co. Ltd. (Shanghai, China). Glass-bottom culture dishes were from Nest Biotechnology Co. Ltd. (Wuxi, China). Deionized water was used in experiments. Unless stated, all reagents were sourced from standard suppliers. All chemicals were of analytical grade and used without further purification.

2.2. Synthesis of Fe_3O_4 MNPs

Fe_3O_4 MNPs with different sizes were synthesized by a modified bi-solvent solvothermal method [42,43]. $FeCl_3$•$6H_2O$ (2.16 g), NaAC (8 g) and PAA (0.3 g) were dissolved in a mixture of DEG and EG (total volume: 80 mL) under magnetic stirring. After vigorous stirring for 1 h, the obtained yellow solution was transferred into a telfton-lined stainless-steel autoclave. Then the autoclave was sealed and heated at 200 °C for 12 h. After cooling to room temperature, the impure Fe_3O_4 MNPs solution were purified by washing 5 times with deionized water and ethanol, respectively, and finally separated from the suspension solution by a magnet. The size of Fe_3O_4 MNPs was controlled by the DEG/EG ratio, with ratios of 76/4 leading to 20 nm, 60/20 leading to 100 nm, and 50/30 leading to 200 nm.

2.3. Preparation of PAAm-Fe_3O_4 magnetic nanocomposite hydrogels

The PAAm-Fe_3O_4 magnetic nanocomposite hydrogels were prepared based on a protocol according to previous reports [30,31] and modified. To enhance adhesion between the dish and the magnetic hydrogel, the glass-bottom culture dish (Supplementary Fig. S1A) was pretreated with APTES solution (4% v/v in water, 2 mL) and glutaraldehyde solution (0.5% v/v in PBS, 2 mL). Solutions of AM (25% w/v in water, 200 μL), BIS (0.1% w/v in water, 100 μL), Fe_3O_4 MNPs, AP (10% w/v in water, 5 μL), and TEMED (1% w/v in water, 1 μL) were mixed in deionized water to synthesize the pre-gel solution (total volume: 1 mL). Then the pre-gel solution (12 μL) was transferred quickly onto the pretreated dish. Subsequently, the light plastic coverslip (diameter: 12 mm) was slowly placed onto

the top of the pre-gel solution droplet without any trapped bubbles. The droplet was squeezed to become flat (Supplementary Fig. S1B) and polymerized at room temperature for 20 min to achieve complete polymerization. With the blending method, the obtained hydrogel, which was about 100 μm of thickness, was fixed in the glass-bottom culture dish. In order to promote cell adhesion on the magnetic hydrogel, collagen type I (0.6% w/v in 6 mM acetic acid) was conjugated to the hydrogel with the heterobifunctional protein cross-linker sulfo-SANPAH (1 mg/mL) which was used to covalently bond the hydrogel to the collagen. Finally, the collagen-modified magnetic hydrogel was stored in the PBS at 4 °C until further cell culture use.

2.4. Pre-structure process

During the preparation of magnetic nanocomposite hydrogels, the pre-gel solutions are cured under MF. In this process, the Fe_3O_4 MNPs are driven by the magnetic force to form chain-like structures in the magnetic hydrogels. This process is called the pre-structure (PS) process [44]. The solenoid coils, which were assembled by an iron core (length: 10 cm, diameter: 4 cm) and a copper coil (diameter: 1 mm, 2000 turns), were used to generate the uniform MF required for the PS process. During the PS process, the pre-gel solution was placed in the groove of the solenoid coils under the electromagnetic field, making sure that the magnetic lines went through the pre-gel solution vertically. In present work, the PS intensity was: 0 (*i.e.* no PS), 50, 100, and 200 mT, respectively, and tunable by an electrical current.

2.5. Characterization

Transmission electron microscopy (TEM) images of Fe_3O_4 MNPs were taken on a JEOL JEM-F200 microscope at an accelerating voltage of 200 kV. The magnetic properties of Fe_3O_4 MNPs were measured on a Quantum Design vibrating sample magnetometer (VSM) at room temperature with the applied field sweeping from −40 to 40 kOe. X-ray diffraction (XRD) powder patterns of the Fe_3O_4 MNPs were obtained on a PHILIPS X'Pert MPD with an angle range of 2θ = 20–80°. Fourier transform infrared (FTIR) spectrometry of the powder samples was tested on a Thermo Nicolet 8700 using potassium bromide in the wavenumber region between 400 and 4000 cm^{-1}. The microstructures of freeze-dried magnetic hydrogels were analyzed by a GeminiSEM 500 scanning electron microscopy (SEM) using an accelerating voltage of 15 kV.

2.6. Dynamic mechanical properties of PAAm-Fe_3O_4 magnetic nanocomposite hydrogels

The dynamic mechanical properties of the PAAm-Fe_3O_4 magnetic nanocomposite hydrogels were measured by a commercial rheometer (Physica MCR 301, Anton Paar Co., Austria) with an MF generator. The MF was generated by an inbuilt coil and the magnetic flux density was controlled by the current. The linear correspondence between current and magnetic flux density was 1A for 240mT (Supplementary Fig. S2). The test sample was placed between the rotating disk and the base with a gap of 1 mm. For oscillatory shear sweep tests, the magnetic flux density linearly increased over time from 0 to 480 mT (corresponding current: 0 to 2 A) at 25 °C. The frequency was 1 Hz and the shear strain amplitude was 5%.

For polymers, the shear modulus (G) in oscillatory shear mode is related to their storage modulus (G') and loss modulus (G") as follows: G = G'+G". When G'>>G", G can be regarded as approximated as G'. The Young's modulus (E) represents the stiffness and is related to shear modulus through Poisson's ratio. Then the correspondence between G' and E is: G' = G = E/[2(1 + ν)]; where ν is the Poisson's ratio of PAAm hydrogel of about 0.48 as reported in previous study [45]. Therefore, the E in present work is about 2.96 times of the G' measured by the rheometer.

2.7. Cell culture

The hMSCs were generously provided by the First Affiliated Hospital of Anhui Medical University (Hefei, Anhui, China) and cultured using a modified protocol according to previous reports [46]. In present work, the cells at passage six or lower were cultured in DMEM containing 10% (v/v) FBS and 1% (v/v) penicillin-streptomycin solution at 37 °C in a humidified atmosphere of 5% CO_2. Before seeding cells, prepared collagen-modified magnetic hydrogels were incubated in PBS overnight and rinsed with PBS. Hydrogels were then sterilized with 254-nm UV light for at least 1 h and incubated in culture medium for 30 min before cell seeding. After hydrogel sterilization, the cells were washed with PBS and then digested from culture flasks by 0.25% (v/v) trypsin-EDTA solution for 5 min. Then the digested cells were centrifuged at 1000 rpm for 5 min. Finally, cells were resuspended and seeded in the prepared collagen-modified magnetic hydrogel for subsequent experiments.

2.8. Cell viability

Cell viability were measured by a fluorescent staining kit of acridine orange/ethidium bromide (AO/EB) (KeyGen BioTECH, China). The detached hMSCs were resuspended in 25 μL of DMEM culture medium and 2 μL of the fluorescent staining solution (100 μg/mL AO and 100 μg/mL EB), then incubated for 5 min at room temperature. The hMSCs were stained with AO for live cells (green) and EB for dead cells (bright red), and observed using an inverted fluorescence microscope (Leica, Germany). Cell viability was calculated as the percentage of live cells to the total number of cells.

2.9. Cell morphology

The bright-field images and fluorescence images of the hMSCs morphology were observed under an inverted fluorescence microscope (Leica, Germany). For the fluorescence images, the hMSCs were fixed with formaldehyde (4% v/v in PBS) for 10 min, and permeabilized with TRITON-X-100 (0.5% v/v in PBS) for 10 min. Then the fixed cells were stained with DAPI (1 μg/mL in PBS) for nucleus and TRITC-phalloidin (2 μg/mL in PBS) for F-actin at 37 °C for 30 min. Furthermore, vinculins were incubated with diluted primary antibody (1:1000 dilution of VCL/Vinculin Rabbit Polyclonal Antibody; Beyotime Biotechnology, Shanghai, China) at 4 °C for 1 h. Then the cells were incubated with secondary antibody (1:1000 dilution of anti-rabbit IgG) in PBS for 1 h at room temperature. Finally, they were imaged by the fluorescence microscopy. The cells were washed 3 times with PBS after every single operation. Quantitative morphometric analyses of the hMSCs such as cell area, cell aspect ratio, and cell circularity, were measured by ImageJ.

2.10. Statistical analysis

All data were presented as mean ± standard deviation. The significance of differences was tested using two-tailed Student's t-tests and a p value less than 0.05 was considered statistically significant.

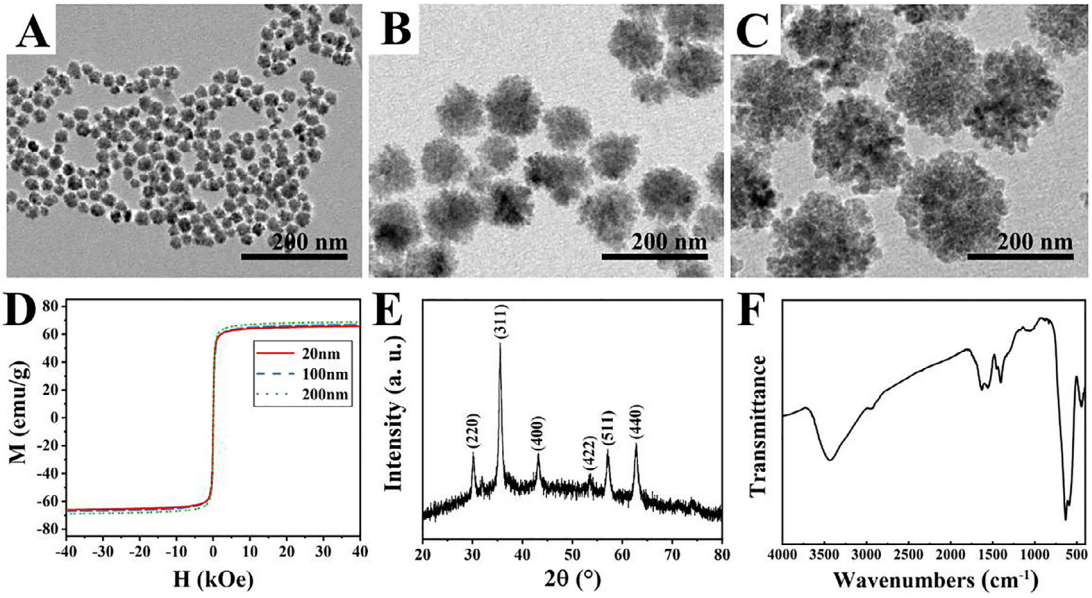

Fig. 1. Characterization of Fe_3O_4 MNPs. **(A–C)** TEM images of Fe_3O_4 MNPs with **(A)** 20, **(B)** 100, and **(C)** 200 nm; **(D)** Hysteresis loops of Fe_3O_4 MNPs with 20, 100, and 200 nm; **(E)** XRD pattern of Fe_3O_4 MNPs with 200 nm; **(E)** FTIR spectrum of Fe_3O_4 MNPs with 200 nm.

3. Results

3.1. Characterization of Fe_3O_4 MNPs

In present work, a modified bi-solvent solvothermal method was used to prepare 20, 100 and 200 nm Fe_3O_4 MNPs [42,43]. As shown in Fig. 1A–C, all the prepared Fe_3O_4 MNPs, which were composed of large amount of tiny nanocrystals, had nearly monodispersed sizes that were tunable by varying the ratio of EG/DEG. Detailed observation of the image of Fe_3O_4 MNPs confirmed that these monodisperse particles displayed a polycrystalline nanostructure. Moreover, the Fe_3O_4 MNPs had narrow size distributions without obvious aggregations and almost uniform spherical shapes, which made them ideal materials for the fabrication of magnetic nanocomposite hydrogels.

To investigate the magnetic properties of the Fe_3O_4 MNPs, the hysteresis loops (Fig. 1D) were measured by a VSM at room temperature. All the magnetization curves were hysteresis-free and smooth which indicated that the coercive force and the residual magnetization were almost zero, confirming that all the prepared Fe_3O_4 MNPs were superparamagnetic. The Fe_3O_4 MNPs of different sizes of 20, 100 and 200 nm had high magnetization with magnetic saturation values of 66, 67, 69 emu/g, respectively. Their similar magnetic characteristics were dependent on the analogous crystalline nanostructure of the Fe_3O_4 MNPs, which played a crucial role in the magnetic characteristics, in agreement with the above TEM analysis.

Fig. 1E showed the XRD pattern of the prepared Fe_3O_4 MNPs with 200 nm. The relative intensity and position of the peaks matched well with the standard Fe_3O_4. In addition, there was no other peak found in the XRD pattern, indicating the purity of the prepared Fe_3O_4 MNPs. The broadened peaks also indicated that the Fe_3O_4 MNPs were consisted of tiny nanocrystals, which agreed with the above analysis.

The FTIR spectrum of Fe_3O_4 MNPs with 200 nm was shown in Fig. 1F. The absorption peak at 581 cm^{-1} was attributed to the stretching vibration of Fe–O. Characteristic peaks COO– symmetric vibration of and COO– asymmetric vibration appeared at 1408 and 1564 cm^{-1}, respectively, suggesting numerous carboxylate groups cooperated with the iron cations [42]. The Fe_3O_4 MNPs would be dispersed into water as stable dispersions because of the existence of such water-soluble polymers.

3.2. Parameters impacting the response of hydrogel stiffness to MF

When a steady, uniform MF was applied to the magnet vulcanized rubber, the magnetic particles in the rubber which stably magnetized could be regarded as magnetic dipoles [47]. Under this assumption of magnetic dipole model, the magnetic particles would tend to arrange a chain-like structure along the direction of MF. The forces that made the particles tend to move towards the chain-like structure would lead a shrinking of the matrix along the field direction [47,48]. These movements of the magnetic particles were significantly influenced by the magnetic interaction forces, excluded-volume repulsive forces, Van der Waals (VDW) forces, and resistance forces [49].

It was assumed that the interaction forces only existed between the adjacent particles, and the particles were aligned along the direction of the MF. For any two neighboring particles i and j with a relative displacement vector r_{ij} in the MF, the magnetic interaction force could be expressed as [49]:

$$F_{ij}^{\text{dipole}} = -\frac{3\mu_0}{4\pi r_{ij}\mu_1} \times \left[\left(m_i \cdot m_j\right)\hat{r} - 5\left(m_i \cdot \hat{r}\right)\left(m_j \cdot \hat{r}\right)\hat{r} + \left(m_j \cdot \hat{r}\right)m_i + \left(m_i \cdot \hat{r}\right)m_j\right] \quad (1)$$

where r_{ij} was the distance between the particles i and j, μ_1 and μ_0 were the permeability of the rubber matrix and vacuum, respectively, and m_i and m_j were the magnetic moments of the magnetic particles i and j, respectively.

To prevent the overlap of the particles, the excluded-volume repulsive force was included, and presented as [49]:

$$F_{ij}^{\text{ev}} = A\frac{3\mu_0 m_i \cdot m_j}{4\pi d_{ij}^4}\exp\left[-\xi\left(r_{ij}/d_{ij} - 1\right)\right]\cdot\widehat{r_{ij}} \quad (2)$$

where d_{ij} was the average particle size of the particles i and j.

When a magnetic particle i moved in the matrix, it would be hampered by the resistance force from the surrounding matrix. The resistance force could be calculated as:

$$F_i^{\text{d}} = -\frac{19}{8}\pi\left(\tau_0 d_i^2\hat{v} + d_i\eta v\right) \quad (3)$$

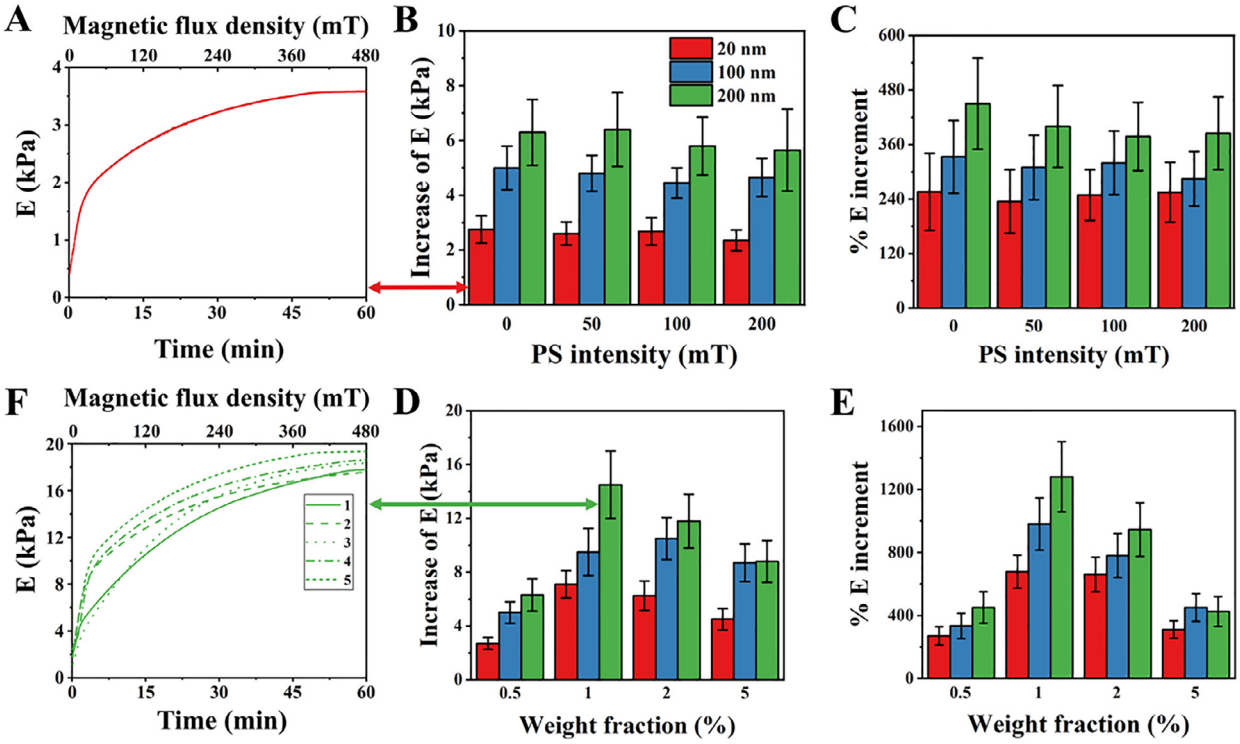

Fig. 2. Dynamic mechanical properties of PAAm-Fe_3O_4 magnetic nanocomposite hydrogels. (A) Curve of magnetic hydrogel stiffness under the application of MF, showing the ability to increase stiffness and the saturation of stiffness (one sample in the red plot in Fig. 2B). The magnetic flux density increased linearly with time from 0 to 480 mT. (B,C) Chart of (B) the increase of stiffness and (C) the rate of stiffness increment of the magnetic hydrogels with the same weight fraction (0.5%), and different particle sizes and different PS intensity. Results were reported as mean ± standard deviation (SD); $n > 20$. (D,E) Chart of (D) the increase of stiffness and (E) the rate of stiffness increment of the magnetic hydrogels with the same PS intensity (0 mT), and different particle sizes and different weight fraction (mean ± SD; $n > 20$). (F) Curves of the stiffness of five optimal samples, indicating the reproducibility (five samples in the green plot in Fig. 2D). (For interpretation of the references to color in this figure legend, the reader is referred to the web version of this article.)

where η was the equivalent viscosity of the matrix, d_i was the particle size of the particle *i*, v is the moving velocity of the particle *i* in the matrix.

In summary, except for the weak VDW forces which can be ignored, the movements of the magnetic particles in the rubber matrix mainly depended on the magnetic interaction force, the excluded-volume repulsive forces, and the resistance forces. Since the elastic behavior of hydrogel was similar to rubber materials, their elasticity could be understood on the basis of the classic theory of rubber elasticity [50]. Thus, the movements of Fe_3O_4 MNPs in the magnetic hydrogels, which varied the stiffness of magnetic hydrogels, also depended on the forces mentioned above. Obviously, the particle size and the spacing between particles (*i.e.* the weight fraction of the magnetic particles) were the variables in the equations above. We therefore speculated that the size and the weight fraction of the Fe_3O_4 MNPs could impact the response of the hydrogel stiffness to the MF. Moreover the effect of pre-structure intensity was also investigated. However, the effect of these factors on the hydrogel stiffness response was not clearly identified. Therefore, our subsequent work was to define the optimal parameters of the magnetic nanocomposite hydrogels to maximize their dynamic mechanical properties.

3.3. Optimal parameters of PAAm-Fe_3O_4 magnetic nanocomposite hydrogels

The evolution of the Young's modulus (E) of the PAAm-Fe_3O_4 magnetic nanocomposite hydrogel (particle size of 20 nm, weight fraction of 0.5%, PS intensity of 0 mT) under the application of MF were monitored (Fig. 2A) by oscillatory shear sweep test. Obviously, an increasing trend of hydrogel stiffness can be observed over time. A sharp increase of hydrogel stiffness was observed when the hydrogel was applied by the MF for the first 20 min, indicating the ability of real-time tunable hydrogel stiffness. After 45 min, the stiffness gradually plateaued, confirming the saturation state of hydrogel stiffness. Overall, it was demonstrated that the hydrogel stiffness could indeed be tuned in real time under the action of MF. We subsequently characterize the PAAm-Fe_3O_4 magnetic nanocomposite hydrogel by FTIR spectroscopy (Supplementary Fig. S3). The magnetic hydrogel revealed the peak at 3415 cm^{-1} corresponding to the O–H stretch. The peak at 3198 cm^{-1} was due to the stretching vibration of N–H. Characteristic peaks of C=O stretching vibration (amide I) and N–H bending vibration (amide II) appeared at 1663 and 1619 cm^{-1}, respectively. The peak at 590 cm^{-1} was ascribed to Fe–O stretching. These results demonstrated that the preparation of the PAAm-Fe_3O_4 magnetic nanocomposite hydrogel was successfully completed.

When an MF is applied to the pre-gel solutions of magnetic hydrogels until the hydrogels are cured, the Fe_3O_4 MNPs in the hydrogels will form a chain-like structure along the direction of the MF, this process is called the pre-structure (PS) process [44]. We conjectured that PS process would cause the Fe_3O_4 MNPs to pre-align, and then reduce their displacement required for their subsequent movement, thus reducing the resistance work and maximizing the increase of hydrogels stiffness. To figure out the effect of PS intensity on the response of hydrogel stiffness to MF, the magnetic hydrogels with same Fe_3O_4 MNPs particle size of 20 nm and same weight fraction of 0.5% were pre-structured with different PS intensities of 0 (*i.e.* no PS), 50, 100, and 200 mT for 20 min at room temperature, respectively. After gel formation, each magnetic hydrogel sample was scanned by a rheometer in a current which linearly enhanced from 0 to 2 A (*i.e.* 0 to 480 mT) for 1 h, re-

spectively. Each condition of experiments was repeated at least 20 times to obtain the increase of stiffness (red plot in Fig. 2B) and the rate of stiffness increment (red plot in Fig. 2C) of the magnetic nanocomposite hydrogels. Interestingly, in contrast to our expectation that PS would enhance the response of magnetic hydrogel stiffness to MF, the increase of stiffness and the rate of stiffness increment hardly changed with the increasing of the PS intensity.

Subsequently, to verify this result, we kept the weight fraction of 0.5% constant and adjusted the particle size of Fe_3O_4 MNPs to 100 and 200 nm. Under these conditions, the magnetic hydrogels were tested with four different PS intensity, respectively. As shown in the blue and green plot in Fig. 2B,C, under the same particle size, the increase of stiffness and the rate of stiffness increment likewise almost unchanged with the PS intensity. We then took the bright-field images and SEM images of the magnetic hydrogels with and without PS (Supplementary Fig. S4) to verify the formation of chain-like structures. The chain-like arrangements of the Fe_3O_4 MNPs inside the magnetic hydrogel with PS process could be easily observed with the naked eyes in the bright-field images. SEM images showed that the magnetic hydrogel with PS process exhibited the chain-like structures consisting of small aggregates of Fe_3O_4 MNPs. These demonstrated the formation of magnetic nanoparticle chains after PS process. Therefore, the lack of significant effect of PS on the stiffness response was not due to the absence of nanoparticle chain formation. The qualitative inferences based on data and observations suggested that the PS intensity did not have a significant influence on the response of the hydrogel stiffness to the MF in our case. We speculated that it may be because the particle size and weight fraction of the Fe_3O_4 MNPs were constant, and the saturation of hydrogel stiffness was due to the magnetization saturation of the Fe_3O_4 MNPs, which made the potential for the increase of hydrogel stiffness also have a saturation state and not be altered by the PS intensity. The PS of 0 mT (*i.e.* no PS) was therefore selected as the optimal condition for subsequent studies.

In order to further investigate the effect of particle size and weight fraction of Fe_3O_4 MNPs on the increase of hydrogel stiffness, the magnetic hydrogels with four different weight fractions (0.5, 1, 2 and 5%) and three different particle sizes (20, 100, and 200 nm) of Fe_3O_4 MNPs were tested, respectively. It was evident that the increase of stiffness (Fig. 2D) and the rate of stiffness increment (Fig. 2E) did not keep enhancing with the increasing weight fraction. Instead, the hydrogels with the weight fraction of 1% as a threshold had the highest stiffness increment in most cases. Because a greater weight fraction of Fe_3O_4 MNPs meant a larger number of Fe_3O_4 MNPs and a smaller distance of Fe_3O_4 MNPs. In other words, a larger weight fraction made the excluded-volume repulsive force larger, and then the hydrogel structure more compact, which inhibited the increase of hydrogel stiffness. This led to an increase of hydrogel stiffness with increasing weight fraction of Fe_3O_4 MNPs up to a threshold value and then decreasing. Hence, the weight fraction of 1% was chosen as the optimal parameter in present work

It was clearly observed that the increase of stiffness (Fig. 2B,D) and the rate of stiffness increment (Fig. 2C,E) of the magnetic hydrogels increased with the particle size of Fe_3O_4 MNPs. This was by reason that the larger size of Fe_3O_4 MNPs led to greater magnetic interactions between the particles of the magnetic hydrogels, thus increasing the response of hydrogel stiffness to MF. However, too large of particle size of Fe_3O_4 MNPs were detrimental to the monodispersity of Fe_3O_4 MNPs and the stability of magnetic hydrogels, which would adversely affect the cell culture. Moreover, hydrogels containing nanoscale particles had been demonstrated to be more suitable for biomedical applications than those with microscale particles [51]. Thus, the particle size of 200 nm was used as the optimal parameter.

In summary, the optimal parameters of magnetic nanocomposite hydrogels were obtained with the PS intensity of 0 mT, the Fe_3O_4 MNPs weight fraction of 1%, and the Fe_3O_4 MNPs particle size of 200 nm, respectively. Subsequently, the stiffness of five optimal samples were measured to evaluate their reproducibility (Fig. 2F). As shown in Fig. 2F, the magnetic hydrogel could provide a wide tunable stiffness range about from 0.3 to 20 kPa, with a high reproducibility. The maximum increase of stiffness and the rate of stiffness increment could be more than 17 kPa and 1500%, respectively. This broad range of adjustable stiffness was almost comparable to most of human tissue elasticity (such as brain, fat, and muscle), demonstrating the ability of this magnetic hydrogel to be a stiffening cell culture platform for multiple types of cells.

3.4. External magnetic field generator

Dynamic mechanical properties of the magnetic hydrogels were measured under the application of a linear increase MF from 0 to 480 mT. However, there were two disadvantages for this MF generator. First, the size of the generator was too large for the incubator to match the requirements of cell culture. Second, it was hardly possible to eliminate the interference of heat and pollution caused by the generator, which adversely affect the culture of hMSCs. For these reasons, a small size permanent magnet (a cylinder with a diameter of 50 mm and height of 30 mm) was used in the cell culture incubator to provide a uniform and constant MF of 240 mT. The simulation of the magnetic flux density was based on the Maxwell's equations and analyzed by COMSOL software (version 5.5) using finite element analysis (Supplementary Fig. S5). The simulation parameters were shown in Supplementary Table S1. It is observed that the field in the magnetic hydrogel region was uniform and the magnetic flux density was about 240 mT, which was consistent with the measured value.

We speculated that there should be no significant difference in the increase of hydrogel stiffness between the two methods of applying MF, because of the same work done on the magnetic hydrogels in these two methods. To verify this speculation, the increase of hydrogel stiffness (not optimal hydrogels) were measured under two methods of applying MF which were linearly enhanced MF from 0 to 480 mT (black curves in Fig. 3B) and maintained at a constant MF of 240 mT (red curves in Fig. 3B), respectively. The quantitative analysis of the increase of hydrogel stiffness (Fig. 3C) showed that there was no significant difference between the two methods. Therefore, it was completely viable to employ a permanent magnet as the external MF generator in the cell culture incubator for subsequent experiments.

Subsequently, to verify that the stiffness of magnetic hydrogels does not be altered with time, but only by MF, the hydrogels were magnetized with a constant MF of 240 mT for 1 h (0–1 h in Fig. 3D), and then the MF generator was turned off for 12 h (1–13 h in Fig. 3D), finally the hydrogel stiffness was measured again (13–14 h in Fig. 3D). It was observed that the stiffness at 1 h was not significantly different from the stiffness at 13 h, and there was almost no change of the stiffness between 13 and 14 h. For the long-term stability, there was no statistical difference in the hydrogel stiffness between any time points during the 15 days culture (Supplementary Fig. S6). These results indicated that the stiffness of the magnetic hydrogel did not change over time after being enhanced to saturation, with good long-term stability, which provided beneficial effects for cell culture.

3.5. Structural characterization of PAAm-Fe_3O_4 magnetic nanocomposite hydrogels

The influence of the application of the MF on the microstructures of PAAm-Fe_3O_4 magnetic nanocomposite hydrogels was ob-

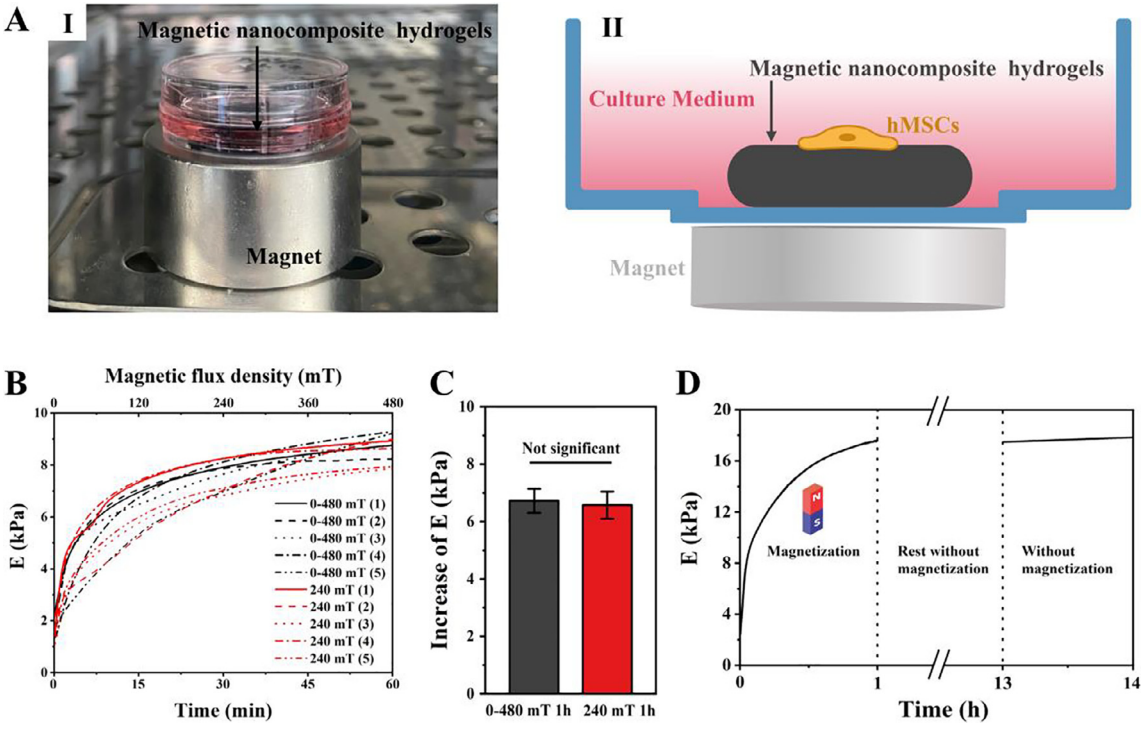

Fig. 3. Application method of external MF. **(A)** (I) Image of the permanent magnet used as the external MF generator in the cell culture incubator. (II) The schematic illustration of hMSCs cultured on collagen-modified magnetic nanocomposite hydrogels. **(B)** Curves of hydrogel stiffness under two application method of MF. The black curves were for the linear increase MF with time from 0 to 480 mT, and the red curves were for the constant MF of 240 mT. **(C)** Plot of the increase of hydrogel stiffness under two methods (mean ± SD; n=10). **(D)** Curve of the stiffness of the magnetic hydrogel which was magnetized by MF for 1 h (0–1 h), and then rest for 12 h (1–13 h), finally tested again (13–14 h), suggesting that the hydrogel stiffness was tuned by MF instead of time. (For interpretation of the references to color in this figure legend, the reader is referred to the web version of this article.)

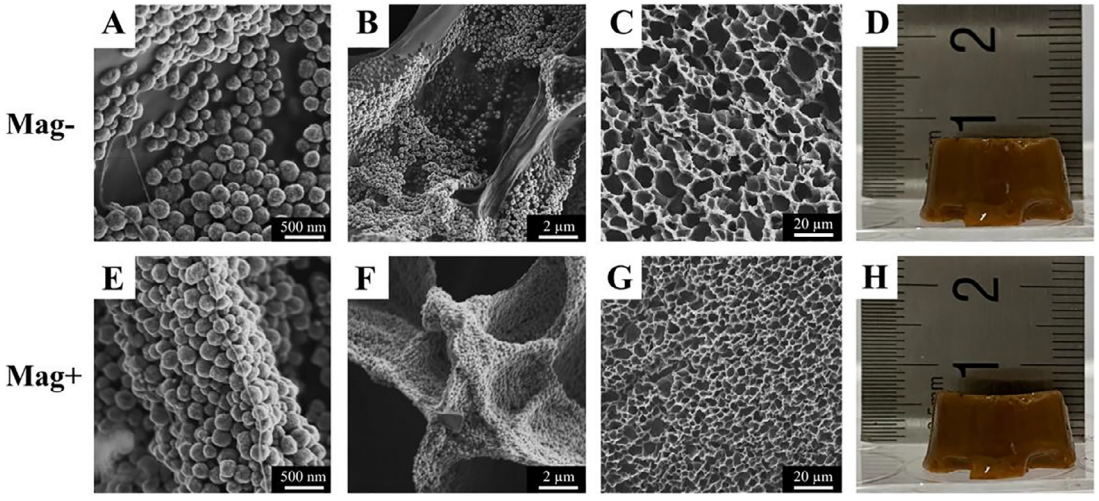

Fig. 4. Structural characterization of PAAm-Fe_3O_4 magnetic nanocomposite hydrogels before (Mag−) and after magnetization (Mag+). SEM images of freeze-dried magnetic hydrogels (A–C) before and (E–G) after magnetization. Photographs of the magnetic hydrogels (D) before and (H) after magnetization.

tained by SEM. Representative SEM images of the freeze-dried magnetic hydrogels before ("Mag-" in Fig. 4A–C) and after ("Mag+" in Fig. 4E–G) magnetization showed that the surface topology of all hydrogels displayed honeycomb-like porous structures, and presented highly analogous structures to hydrogels. Moreover, we observed significant differences in pore sizes, which was inversely correlated with stiffness. After magnetization, the arrangements of Fe_3O_4 MNPs exhibited ordered tight structures, whereas in the absence of the magnetization, Fe_3O_4 MNPs exhibited random and disorganized microstructures. For the macrostructures, the volume of magnetic hydrogel reduced by nearly 20% after magnetization (Fig. 4D,H), indicating that the alteration in microstructure could lead to the variation in macroscopic volume.

Due to the action of MF, the Fe_3O_4 MNPs in the magnetic nanocomposite hydrogels were attracted to close to each other, and tended to align chain-like structures in the direction of MF, thereby squeezing the polymer chains, thus narrowing the spacing of the polymer chains, then making the pore size smaller, and resulting in a smaller volume and greater stiffness of the magnetic hydrogels. Remarkably, the pore sizes observed by SEM of the freeze-dried hydrogels may not represent the actual pore sizes in the hydrated state. But it would reveal the mechanism of the variation

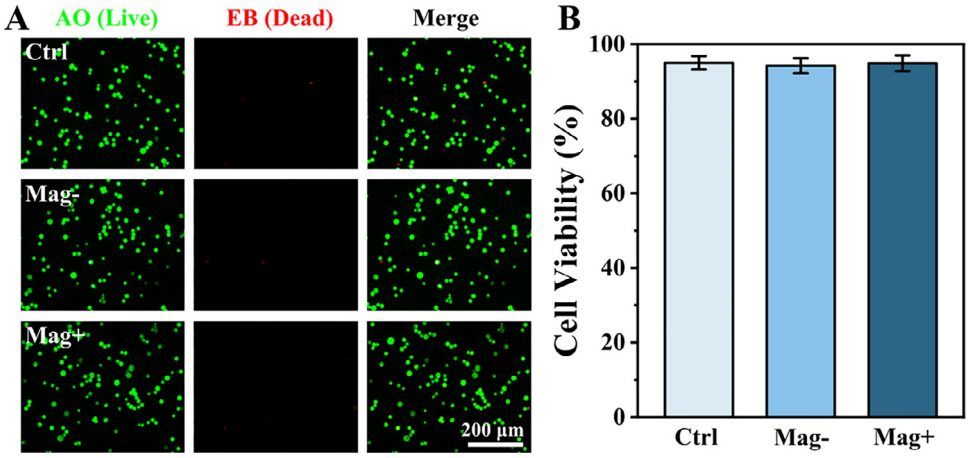

Fig. 5. The biocompatibility of PAAm-Fe_3O_4 magnetic nanocomposite hydrogels. (A) Fluorescence images showing viability of hMSCs under three conditions. (Ctrl): hMSCs cultured on Petri dishes (*i.e.* no magnetic hydrogels) and not subjected to magnetization. (Mag−): hMSCs cultured on magnetic hydrogels before magnetization. (Mag+): hMSCs cultured on magnetic hydrogels after magnetization. The hMSCs were stained with AO for live cells (green) and with EB for dead cells (bright red). (B) Cell viability (*i.e.* the ratios of live cells to the total cells) of hMSCs under aforementioned conditions (mean ± SD; $n = 8$). (For interpretation of the references to color in this figure legend, the reader is referred to the web version of this article.)

of hydrogel stiffness and the relationship between pore size and stiffness.

3.6. Biocompatibility of PAAm-Fe_3O_4 magnetic nanocomposite hydrogels

The primary hMSCs were investigated in present work because of their excellent capabilities of self-renewal and multi-lineage differentiation, and widely applied in medical and tissue engineering applications [46]. However, the primary hMSCs were so sensitive to their culture environment that they required the substrates with high biocompatibility. Hence, it was necessary to identify the extent of the influence of magnetic hydrogels and magnetization on the viability of hMSCs. The hMSCs cultured on collagen-modified magnetic hydrogels before ("Mag−") and after magnetization ("Mag+") were therefore evaluated for their viability by a fluorescent staining kit of AO/EB, respectively, where the green fluorescence of AO represented live cells and the bright red fluorescence of EB represented dead cells. Remarkably, the dark red fluorescence was not representative of dead cells.

As shown in Fig. 5A, it could be observed that there was no significant difference in the viability of the hMSCs between the two experimental groups ("Mag−" and "Mag+") and the control group ("Ctrl") that was cultured on Petri dishes without magnetic hydrogels and not subjected to magnetization. The ratios of live cells to the total cells under three conditions were all over 90% (Fig. 5B), thereby indicating excellent biocompatibility of the magnetic hydrogels. These results demonstrated that hMSCs cultured on the collagen-modified magnetic hydrogels before and after magnetization could maintain high viability, which was vital for further cell culture.

3.7. PAAm-Fe_3O_4 Magnetic nanocomposite hydrogels with tunable stiffness for regulating hMSCs morphology

Once the biocompatibility of PAAm-Fe_3O_4 magnetic nanocomposite hydrogels was determined, the next step of investigation was to identify that the morphology of hMSCs was regulated by the variation of hydrogel stiffness, rather than the MF itself. The hMSCs were therefore cultivated on Petri dishes (*i.e.* no magnetic hydrogels) with magnetization for 1 h to assay the impact of MF on the cell morphology. It was shown that there was no significant difference in the morphologies of hMSCs before and after magnetization (Fig. 6A), confirming that MF itself did not influence the morphology of hMSCs.

To explore further the intrinsic correspondence between hMSCs morphology and the tunable stiffness of magnetic hydrogels, the hMSCs were assayed under four different culture conditions (two experimental groups and two control groups) by the following protocol, respectively (Fig. 6B). As mentioned above, the stiffness of optimal magnetic hydrogel before and after magnetization were about 2 kPa and 20 kPa, respectively. Therefore, the hMSCs were cultured on the collagen-modified magnetic hydrogel without magnetization for 48 h, with a constant stiffness of about 20 kPa, as the stiff control group (Ctrl_stiff). For another control group, the hMSCs were seeded on the hydrogel without magnetization for 48 h, with a constant stiffness of about 2 kPa, as the soft control group (Ctrl_soft). For the experimental groups, after 12 h of incubation, the hydrogel was magnetized for 1 h, as an experimental group (12h_Mag+). The hydrogel was magnetized for 1 h after 24 h of incubation, as another experimental group (24h_Mag+). For all samples, the bright-field images were taken every 12 h, and fluorescence images were taken after 48 h of incubation, which the green and blue fluorescence represented F-actin and nucleus, respectively (Fig. 6C).

Since the control hydrogels (Ctrl_stiff) and (Ctrl_soft) were not applied by MF, the hydrogel stiffness had kept constant. As a result, the morphology of hMSCs under both conditions did not change significantly over time. The hMSCs on (Ctrl_stiff) were branched, spindle, or polygonal shapes, because the cells were cultured on a stiffer substrate. In contrast, the hMSCs on (Ctrl_soft) were small and rounded due to cultivation on a softer substrate. These results were consistent with the previous studies [1,3,4]. For the experimental groups (12h_Mag+) and (24h_Mag+), the hMSCs spread significantly over time due to the increase stiffness caused by the magnetization at the corresponding time. The cell area increased and the hMSCs gradually spread from rounded to branched, which showed the typical stem cell morphology on substrates with different stiffness. Overall, the cell morphology was regulated only after the time of application of MF, indicating that it was not until hMSCs sensed the variation of the hydrogel stiffness that their morphologies were regulated.

To investigate further the impact of tunable stiffness on the cell morphology, the morphology of hMSCs under four different culture conditions were subject to quantitative morphometric analysis (Fig. 6D). Since the stiffness of the hydrogels (Ctrl_stiff) and

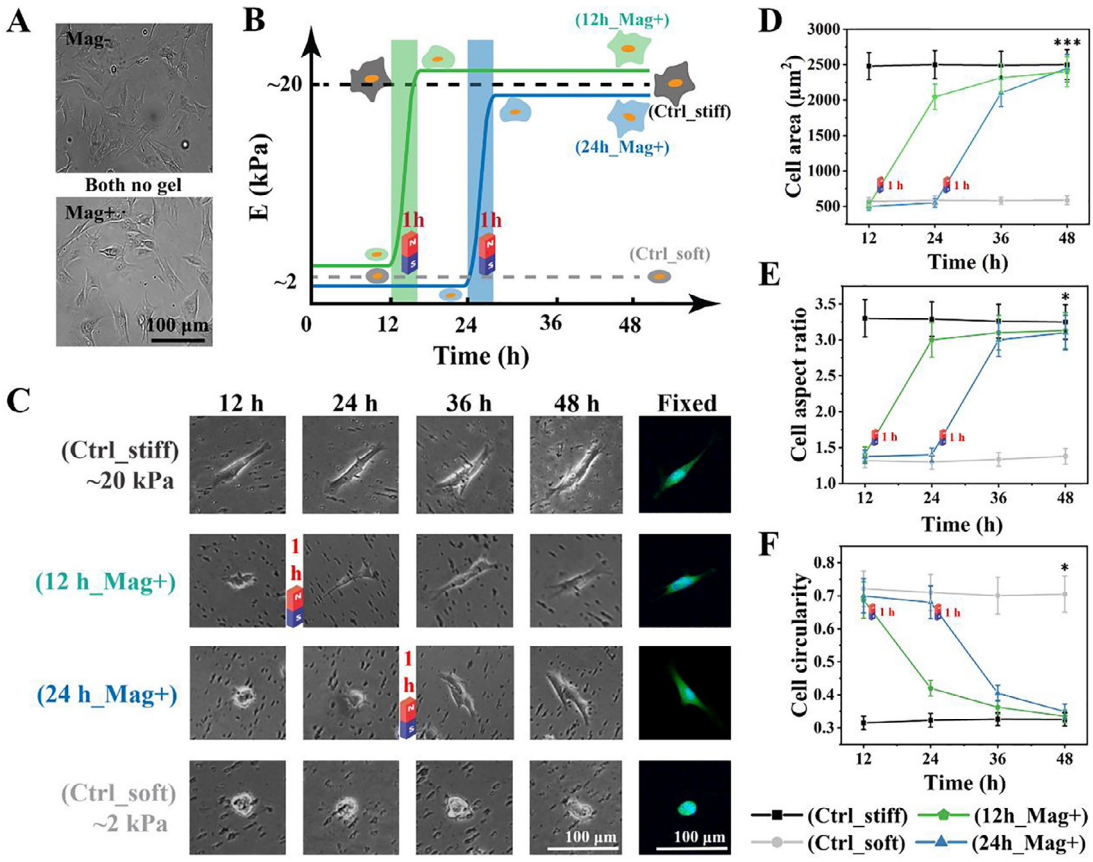

Fig. 6. The morphology of hMSCs regulated by the PAAm-Fe_3O_4 magnetic nanocomposite hydrogels with tunable stiffness. **(A)** Bright field images of hMSCs cultivated on Petri dishes (*i.e.* no magnetic hydrogels) before (Mag−) and after (Mag+) magnetization, suggesting that MF itself did not influence the morphology of hMSCs. **(B)** Schematic diagram of hMSCs cultured on collagen-modified magnetic hydrogels under four different culture conditions. (Ctrl_stiff): constant stiffness of about 20 kPa for 48 h without magnetization. (Ctrl_soft): constant stiffness of about 2 kPa for 48 h without magnetization. (12h_Mag+): magnetized for 1 h after 12 h of incubation. (24h_Mag+): magnetized for 1 h after 24 h of incubation. **(C)** Bright field images and fluorescence images of hMSCs cultured under aforementioned conditions. The hMSCs were fixed after 48 h of incubation and then stained for nucleus (blue) and F-actin (green). The time of application of MF was marked in red. **(D–F)** Quantification of the **(D)** cell area, **(E)** the cell aspect ratio (*i.e.* the ratio of the long side to the short side of the cell), and **(F)** the cell circularity (*i.e.* the ratio of 4π times the area to the square of the perimeter). Results are reported as mean± SD. $n > 200$ cells from 10 different hydrogels. $^{*}p < 0.05$, $^{**}p < 0.01$ and $^{***}p < 0.001$. (For interpretation of the references to color in this figure legend, the reader is referred to the web version of this article.)

(Ctrl_soft) did not change, the cell area remained essentially constant of 2508 ± 223 μm^2 and 593 ± 59 μm^2, respectively. For the hMSCs cultured on (12h_Mag+) and (24h_Mag+), their morphology did not alter significantly until the MF was applied. After applying the MF for 1 h at the corresponding time, the cell area increased to 2422 ± 210 μm^2 on (12h_Mag+) and 2453 ± 196 μm^2 on (24h_Mag+) due to the enhanced stiffness, respectively. Furthermore, after 48 h of incubation, the cell aspect ratios (*i.e.* the ratio of the long diagonal to the short diagonal of the cell) on (12h_Mag+) and (24h_Mag+) increased significantly compared to that on (Ctrl_soft) (Fig. 6E). As for the cell circularities (*i.e.* the ratio of 4π times the area to the square of the perimeter) on (12h_Mag+) and (24h_Mag+) were remarkably lower than that on (Ctrl_soft) (Fig. 6F). These variations of cell morphology were consistent with the responses of hMSCs morphology to matrix stiffening as previously reported [22,28]. All these results confirmed that the morphology of hMSCs could be regulated by the magnetic nanocomposite hydrogels with tunable stiffness.

As demonstrated in previous studies, maturation of focal adhesions (FAs) and F-actin assembly were the primary factors leading to variations of cell morphology [52–54]. Accordingly, we hypothesized that greater hydrogel stiffness caused by the magnetization could facilitate maturation of FAs and F-actin assembly, thus regulating cell morphology. Therefore, to explore the potential mechanisms of matrix stiffening for regulating hMSCs morphology, the expression of FAs and F-actins of the hMSCs cultured on the magnetic hydrogels before and after magnetization were evaluated, respectively (Fig. 7A), where vinculin, a critical component of FAs, was stained to assess the FAs expression. The staining results indicated that hMSCs cultured on the magnetic hydrogels after magnetization exhibited more area of F-actins and FAs than that before magnetization (Fig. 7B,C), implying that stiffer magnetic hydrogels caused by magnetization facilitated the F-actin assembly, and vinculin recruitment and connection to F-actins, resulting in stronger cell adhesion, ultimately regulating cell morphology (Fig. 7D).

4. Discussion

Stiffening hydrogels are of interest in biomedical applications for wound healing, tissue engineering, disease progression, and stem cell therapy. It has been reported that several hydrogel systems can alter their stiffness in response to various stimuli, such as temperature, pH, and light [16–19,22–26,28]. However, there are still some potential interferences with cellular biological behaviors or limitations of tunable stiffness for these hydrogels. To address these problems, we developed a stiffening system based on PAAm-Fe_3O_4 magnetic nanocomposite hydrogel that possessed a relatively wide range of adjustable stiffness and did not adversely affect cell behavior. In this way, such stiffening hydrogel system could simulate the dynamic mechanical environment for probing

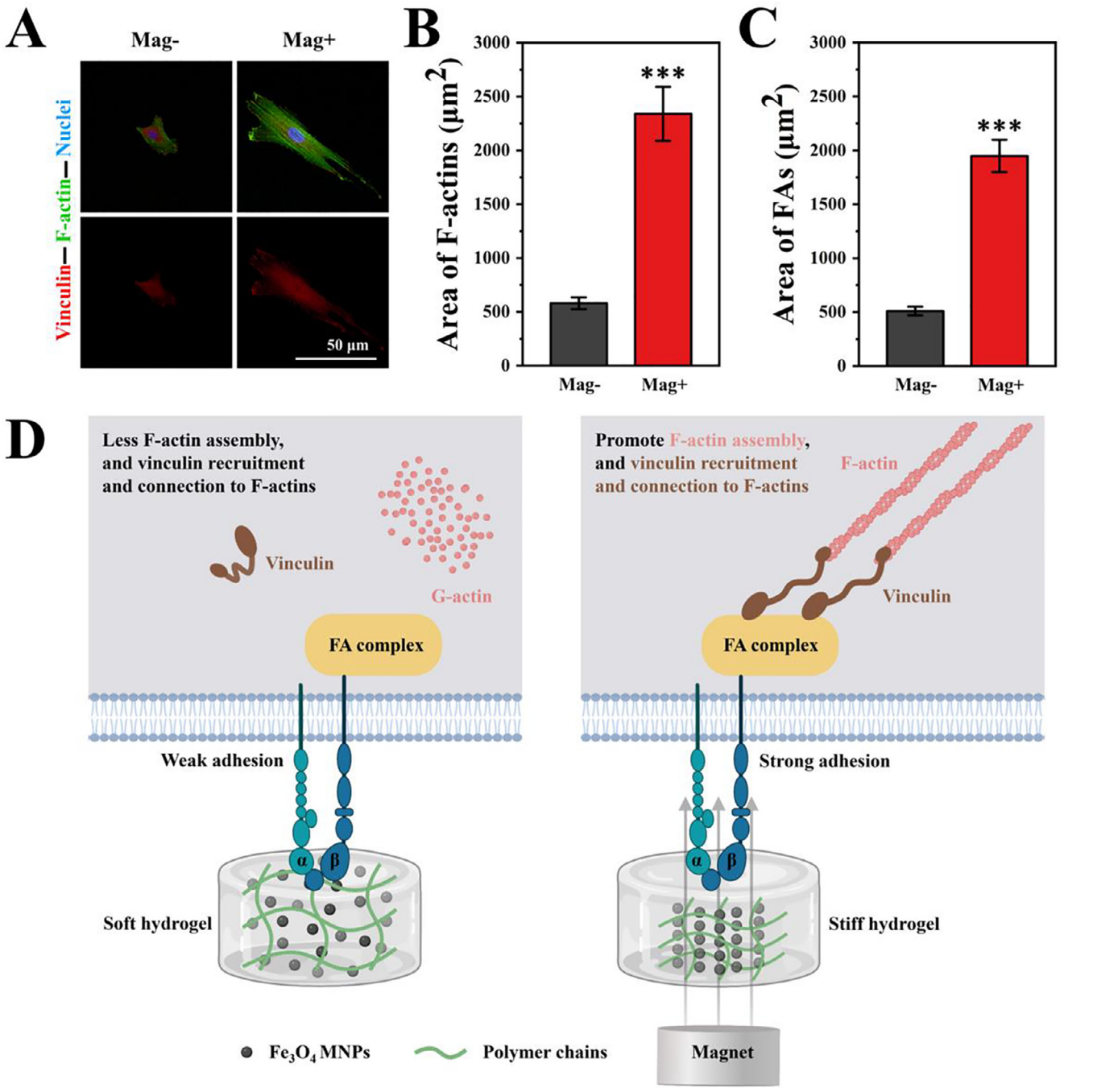

Fig. 7. Potential mechanisms of matrix stiffening to regulate the cell morphology. (A) Fluorescence images of hMSCs cultured on magnetic hydrogels before (Mag−) and after magnetization (Mag+). The hMSCs were stained for F-actins (green), nucleus (blue), and vinculins (red) were stained to assess the area of focal adhesions (FAs). (B,C) Quantification of the area of (B) F-actins and (C) FAs. Results are reported as mean± SD; $n = 5$. $^{*}p < 0.05$, $^{**}p < 0.01$ and $^{***}p < 0.001$. (D) Schematic diagram of the potential mechanism of matrix stiffening for regulating hMSCs morphology. After magnetization, the Fe_3O_4 MNPs in the hydrogels were tended to align chain-like structures in the direction of MF, leading to a smaller spacing of the polymer chains, thereby making the hydrogel stiffness greater. Such greater hydrogel stiffness facilitated vinculin recruitment and connection to F-actins, and F-actin assembly, resulting in stronger adhesion, thus leading to significant spreading of hMSCs with larger area. (For interpretation of the references to color in this figure legend, the reader is referred to the web version of this article.)

cellular responses to matrix stiffening and studying dynamic biological processes.

In present study, we used a modified bi-solvent solvothermal method to prepare monodisperse Fe_3O_4 MNPs with different sizes. We then crosslinked the mixture of Fe_3O_4 MNPs and PAAm pre-gel solution to obtain the PAAm-Fe_3O_4 magnetic nanocomposite hydrogel. The stiffness of the magnetic hydrogel would increase under the action of the MF due to the enhancement of the magnetic interactions of the Fe_3O_4 MNPs. Although our magnetic nanocomposite hydrogel only provided increased stiffening, and the hydrogel stiffness would remain at saturation and not fall back to the baseline level after removing the MF due to the nondispersible magnetic nanoparticles aggregates, it provided the required constant stiffness for subsequent cell culture. Actually, it was beneficial for cell culture to maintain saturated stiffness after removal of MF. If the hydrogel stiffness remains constant only when the MF is applied, a long period of MF sustained application time may have an undesired effect on the cellular behavior.

In order to obtain the optimal parameters of the magnetic hydrogels, we investigated the effect of the PS intensity, the Fe_3O_4 MNPs particle size, and Fe_3O_4 MNPs weight fraction on hydrogel stiffness response to MF. We qualitatively inferred from the data and observations that in our case, the PS intensity had no significant effect on the enhancement of stiffness; the Fe_3O_4 MNPs weight fraction of 1% as a threshold had the highest stiffness increment; the hydrogel stiffness response would increase with the increasing particle size of Fe_3O_4 MNPs in an appropriate range. As a result, the range of stiffness was about 0.3 to 20 kPa, indicating the capacity of magnetic nanocomposite hydrogel for probing the cellular response to matrix stiffening. Overall, the increased magnetic interaction between Fe_3O_4 MNPs due to the action of MF caused Fe_3O_4 MNPs to attract close to each other and tend to arrange a chain-like structure along the direction of MF, which squeezed the polymer chains and thus reduced the polymer chain spacing, resulting in smaller pore sizes and greater hydrogel stiffness.

For cell culture considerations, we employed a small size permanent magnet as the external MF generator to provide a uniform and constant MF of 240 mT, and verified that the magnetic hydrogels possessed excellent biocompatibility. To demonstrate the utility of our stiffening hydrogel system, we investigated the cellular response to dynamic stiffening under four different culture conditions by the protocol. Due to the increasing stiffness induced by magnetization at the corresponding time, the cell area increased obviously with time and the hMSCs gradually spread from rounded to branched. In addition the cell aspect ratio and cell circularity also varied accordingly to the matrix stiffening. These cellular responses were attributed to magnetization-induced hydrogel stiffening, which promoted the assembly of F-actin, the recruitment of vinculin, and vinculin attachment to F-actins, thus leading to stronger cell adhesion. It is demonstrated that this stiffening platform was capable of providing valuable insight into cellular mechanobiological responses.

In the future, the ability of magnetic nanocomposite hydrogels to dynamically controlled mechanical properties using safe MF could be helpful for various biomedical researches. For example, this stiffening biomaterial can simulate the dynamic biomechanical properties *in vivo* to study disease progression and facilitate its applications in wound healing and tissue engineering. Besides, this cell culture platform can be used to direct cell proliferation, migration, and differentiation by modulating its mechanics, mechanotransduction signaling, and ligand distribution (*e.g.*, ligand spacing, ligand tethering and ligand mobility).

5. Conclusion

In summary, we demonstrated that with the pre-structure intensity of 0 mT, the Fe_3O_4 MNPs weight fraction of 1%, and the Fe_3O_4 MNPs particle size of 200 nm, it is possible to obtain the polyacrylamide-Fe_3O_4 magnetic nanocomposite hydrogel with the optimal response of the hydrogel stiffness to magnetic field, which had a wide tunable stiffness range of about 0.3–20 kPa (similar to the stiffness range of most human tissue), a maximum stiffness increase of more than 17 kPa, and a maximum rate of stiffness increment of over 1500%. Such matrix stiffening caused by enhanced magnetic interaction between Fe_3O_4 MNPs by magnetic field could induce the morphological variations of hMSCs cultured on the magnetic hydrogels. Overall, our stiffening cell culture platform not only provided valuable insights into the role of matrix stiffening as a biological behavior regulator of stem cells, but also allowed for better simulation of biomechanical properties of human tissues to investigate dynamic biological processes and facilitate its applications in the biomedical field.

Declaration of Competing Interest

The authors declare no competing financial interests.

CRediT authorship contribution statement

Tianhao Yan: Conceptualization, Data curation, Writing – original draft, Methodology. **Depeng Rao:** Methodology. **Ye Chen:** Methodology. **Yu Wang:** Methodology. **Qingchuan Zhang:** Conceptualization, Writing – original draft. **Shangquan Wu:** Conceptualization, Data curation, Writing – original draft.

Acknowledgments

The authors gratefully acknowledge financial support from the National Natural Science Foundation of China (Grant Nos. 11627803, 11872355, and 12072339) and the Strategic Priority Research Program of the Chinese Academy of Sciences (XDB22040502).

Supplementary materials

Supplementary material associated with this article can be found, in the online version, at doi:10.1016/j.actbio.2021.11.001.

References

[1] A.J. Engler, S. Sen, H.L. Sweeney, D.E. Discher, Matrix elasticity directs stem cell lineage specification, Cell 126 (4) (2006) 677–689.
[2] D. Mitrossilis, J. Fouchard, D. Pereira, F. Postic, A. Richert, M. Saint-Jean, A. Asnacios, Real-time single-cell response to stiffness, Proc. Natl. Acad. Sci. U.S.A. 107 (38) (2010) 16518–16523.
[3] K. Xie, Y. Yang, H. Jiang, Controlling cellular volume via mechanical and physical properties of substrate, Biophys. J. 114 (3) (2018) 675–687.
[4] S. Modaresi, S. Pacelli, J. Whitlow, A. Paul, Deciphering the role of substrate stiffness in enhancing the internalization efficiency of plasmid DNA in stem cells using lipid-based nanocarriers, Nanoscale 10 (19) (2018) 8947–8952.
[5] S.H. Oh, D.B. An, T.H. Kim, J.H. Lee, Wide-range stiffness gradient PVA/HA hydrogel to investigate stem cell differentiation behavior, Acta Biomater. 35 (2016) 23–31.
[6] A. Islam, T. Mbimba, M. Younesi, O. Akkus, Effects of substrate stiffness on the tenoinduction of human mesenchymal stem cells, Acta Biomater. 58 (2017) 244–253.
[7] Y. Yang, X. Wang, X. Hu, N. Kawazoe, Y. Yang, G. Chen, Influence of cell morphology on mesenchymal stem cell transfection, ACS Appl. Mater. Interfaces 11 (2) (2019) 1932–1941.
[8] H. Seong, S.G. Higgins, J. Penders, J.P.K. Armstrong, S.W. Crowder, A.C. Moore, J.E. Sero, M. Becce, M.M. Stevens, Size-tunable nanoneedle arrays for influencing stem cell morphology, gene expression, and nuclear membrane curvature, Acs Nano 14 (5) (2020) 5371–5381.
[9] M.D. Treiser, E.H. Yang, S. Gordonov, D.M. Cohen, I.P. Androulakis, J. Kohn, C.S. Chen, P.V. Moghe, Cytoskeleton-based forecasting of stem cell lineage fates, Proc. Natl. Acad. Sci. U.S.A. 107 (2) (2010) 610–615.
[10] M.D. Cabezas, B. Meckes, C.A. Mirkin, M. Mrksich, Subcellular control over focal adhesion anisotropy, independent of cell morphology, dictates stem cell fate, Acs Nano 13 (10) (2019) 11144–11152.
[11] G. Abagnale, M. Steger, V.H. Nguyen, N. Hersch, A. Sechi, S. Joussen, B. Denecke, R. Merkel, B. Hoffmann, A. Dreser, U. Schnakenberg, A. Gillner, W. Wagner, Surface topography enhances differentiation of mesenchymal stem cells towards osteogenic and adipogenic lineages, Biomaterials 61 (2015) 316–326.
[12] S. Majkut, T. Idema, J. Swift, C. Krieger, A. Liu, D.E. Discher, Heart-specific stiffening in early embryos parallels matrix and myosin expression to optimize beating, Curr. Biol. 23 (23) (2013) 2434–2439.
[13] J.D. Humphrey, E.R. Dufresne, M.A. Schwartz, Mechanotransduction and extracellular matrix homeostasis, Nat. Rev. Mol. Cell Biol. 15 (12) (2014) 802–812.
[14] M. Breitbach, T. Bostani, W. Roell, Y. Xia, O. Dewald, J.M. Nygren, J.W. Fries, K. Tiemann, H. Bohlen, J. Hescheler, A. Welz, W. Bloch, S.E. Jacobsen, B.K. Fleischmann, Potential risks of bone marrow cell transplantation into infarcted hearts, Blood 110 (4) (2007) 1362–1369.
[15] K.R. Levental, H. Yu, L. Kass, J.N. Lakins, M. Egeblad, J.T. Erler, S.F. Fong, K. Csiszar, A. Giaccia, W. Weninger, M. Yamauchi, D.L. Gasser, V.M. Weaver, Matrix crosslinking forces tumor progression by enhancing integrin signaling, Cell 139 (5) (2009) 891–906.
[16] S. Hackelbusch, T. Rossow, D. Steinhilber, D.A. Weitz, S. Seiffert, Hybrid microgels with thermo-tunable elasticity for controllable cell confinement, Adv. Healthc. Mater. 4 (12) (2015) 1841–1848.
[17] W.H. Rombouts, D.W. de Kort, T.T. Pham, C.P. van Mierlo, M.W. Werten, F.A. de Wolf, J. van der Gucht, Reversible temperature-switching of hydrogel stiffness

of coassembled, silk-collagen-like hydrogels, Biomacromolecules 16 (8) (2015) 2506–2513.
[18] H.Y. Yoshikawa, F.F. Rossetti, S. Kaufmann, T. Kaindl, J. Madsen, U. Engel, A.L. Lewis, S.P. Armes, M. Tanaka, Quantitative evaluation of mechanosensing of cells on dynamically tunable hydrogels, J. Am. Chem. Soc. 133 (5) (2011) 1367–1374.
[19] F. Bossard, T. Aubry, G. Gotzamanis, C. Tsitsilianis, pH-Tunable rheological properties of a telechelic cationic polyelectrolyte reversible hydrogel, Soft Matter 2 (6) (2006) 510–516.
[20] T.R. Arnett, Extracellular pH regulates bone cell function, J. Nutr. 138 (2) (2008) 415S–418S.
[21] C.R. Kruse, M. Singh, S. Targosinski, I. Sinha, J.A. Sorensen, E. Eriksson, K. Nuutila, The effect of pH on cell viability, cell migration, cell proliferation, wound closure, and wound reepithelialization: *in vitro* and *in vivo* study, Wound Repair Regen. 25 (2) (2017) 260–269.
[22] M. Guvendiren, J.A. Burdick, Stiffening hydrogels to probe short- and long-term cellular responses to dynamic mechanics, Nat. Commun. 3 (2012) 792.
[23] C. Yang, F.W. DelRio, H. Ma, A.R. Killaars, L.P. Basta, K.A. Kyburz, K.S. Anseth, Spatially patterned matrix elasticity directs stem cell fate, Proc. Natl. Acad. Sci. U.S.A. 113 (31) (2016) E4439–E4445.
[24] R.S. Stowers, S.C. Allen, L.J. Suggs, Dynamic phototuning of 3D hydrogel stiffness, Proc. Natl. Acad. Sci. U.S.A. 112 (7) (2015) 1953–1958.
[25] S. Khetan, M. Guvendiren, W.R. Legant, D.M. Cohen, C.S. Chen, J.A. Burdick, Degradation-mediated cellular traction directs stem cell fate in covalently crosslinked three-dimensional hydrogels, Nat. Mater. 12 (5) (2013) 458–465.
[26] A.M. Rosales, S.L. Vega, F.W. DelRio, J.A. Burdick, K.S. Anseth, Hydrogels with reversible mechanics to probe dynamic cell microenvironments, Angew. Chem. Int. Ed. Engl. 56 (40) (2017) 12132–12136.
[27] M. Lysetska, A. Knoll, D. Boehringer, T. Hey, G. Krauss, G. Krausch, UV light–damaged DNA and its interaction with human replication protein a: an atomic force microscopy study, Nucleic Acids Res. 30 (12) (2002) 2686–2691.
[28] I.N. Lee, O. Dobre, D. Richards, C. Ballestrem, J.M. Curran, J.A. Hunt, S.M. Richardson, J. Swift, L.S. Wong, Photoresponsive hydrogels with photoswitchable mechanical properties allow time-resolved analysis of cellular responses to matrix stiffening, ACS Appl. Mater. Interfaces 10 (9) (2018) 7765–7776.
[29] K. Ogawa, Y. Kuse, K. Tsuruma, S. Kobayashi, M. Shimazawa, H. Hara, Protective effects of bilberry and lingonberry extracts against blue light-emitting diode light-induced retinal photoreceptor cell damage *in vitro*, BMC Complement. Altern. Med. 14 (2014) 120.
[30] J.R. Tse, A.J. Engler, Preparation of hydrogel substrates with tunable mechanical properties, Curr. Protoc. Cell Biol. 47 (1) (2010) 10–16.
[31] Y. Liu, J. Wang, Y. Su, X. Xu, H. Liu, K. Mei, S. Lan, S. Zhang, X. Wu, Y. Cao, Quantifying 3D cell-matrix interactions during mitosis and the effect of anticancer drugs on the interactions, Nano Res. (2021) 1–10.
[32] M.W. Tibbitt, K.S. Anseth, Hydrogels as extracellular matrix mimics for 3D cell culture, Biotechnol. Bioeng. 103 (4) (2009) 655–663.
[33] M.C. Cushing, K.S. Anseth, Materials science. Hydrogel cell cultures, Science 316 (5828) (2007) 1133–1134.
[34] H. Geckil, F. Xu, X. Zhang, S. Moon, U. Demirci, Engineering hydrogels as extracellular matrix mimics, Nanomedicine 5 (3) (2010) 469–484.
[35] Y. Li, G. Huang, X. Zhang, B. Li, Y. Chen, T. Lu, T.J. Lu, F. Xu, Magnetic hydrogels and their potential biomedical applications, Adv. Funct. Mater. 23 (6) (2013) 660–672.
[36] K. Hu, J. Sun, Z. Guo, P. Wang, Q. Chen, M. Ma, N. Gu, A novel magnetic hydrogel with aligned magnetic colloidal assemblies showing controllable enhancement of magnetothermal effect in the presence of alternating magnetic field, Adv. Mater. 27 (15) (2015) 2507–2514.
[37] Y.L. Liu, D. Chen, P. Shang, D.C. Yin, A review of magnet systems for targeted drug delivery, J. Control. Release 302 (2019) 90–104.
[38] A. Pardo, M. Gomez-Florit, S. Barbosa, P. Taboada, R.M.A. Domingues, M.E. Gomes, Magnetic nanocomposite hydrogels for tissue engineering: design concepts and remote actuation strategies to control cell fate, ACS Nano 15 (1) (2021) 175–209.
[39] Y. Cao, M. Hassan, Y. Cheng, Z. Chen, M. Wang, X. Zhang, Z. Haider, G. Zhao, Multifunctional photo- and magnetoresponsive graphene oxide-Fe_3O_4 nanocomposite-alginate hydrogel platform for ice recrystallization inhibition, ACS Appl. Mater. Interfaces 11 (13) (2019) 12379–12388.
[40] F. Gao, W. Xie, Y. Miao, D. Wang, Z. Guo, A. Ghosal, Y. Li, Y. Wei, S.S. Feng, L. Zhao, H.M. Fan, Magnetic hydrogel with optimally adaptive functions for breast cancer recurrence prevention, Adv. Healthc. Mater. 8 (14) (2019) e1900203.
[41] L. Pang, X.F. Dong, C.G. Niu, M. Qi, Dynamic viscoelasticity and magnetorheological property of magnetic hydrogels, J. Magn. Magn. Mater. 498 (2020) 166140.
[42] J. Wu, L. Pei, S. Xuan, Q. Yan, X. Gong, Particle size dependent rheological property in magnetic fluid, J. Magn. Magn. Mater. 408 (2016) 18–25.
[43] S. Xuan, F. Wang, Y.-X.J. Wang, C.Y. Jimmy, K.C.-F. Leung, Facile synthesis of size-controllable monodispersed ferrite nanospheres, J. Mater. Chem. 20 (24) (2010) 5086–5094.
[44] J.F. Li, X.L. Gong, Z.B. Xu, W.Q. Jiang, The effect of pre-structure process on magnetorheological elastomer performance, Int. J. Mater. Res. 99 (12) (2008) 1358–1364.
[45] T. Boudou, J. Ohayon, C. Picart, P. Tracqui, An extended relationship for the characterization of Young's modulus and Poisson's ratio of tunable polyacrylamide gels, Biorheology 43 (6) (2006) 721–728.
[46] J. Wang, G. Zhao, Z. Zhang, X. Xu, X. He, Magnetic induction heating of superparamagnetic nanoparticles during rewarming augments the recovery of hUCM-MSCs cryopreserved by vitrification, Acta Biomater. 33 (2016) 264–274.
[47] J. Feng, S. Xuan, T. Liu, L. Ge, L. Yan, H. Zhou, X. Gong, The prestress-dependent mechanical response of magnetorheological elastomers, Smart Mater. Struct. 24 (8) (2015) 085032.
[48] X. Ruan, Y. Wang, S. Xuan, X. Gong, Magnetic field dependent electric conductivity of the magnetorheological fluids: the influence of oscillatory shear, Smart Mater. Struct. 26 (3) (2017) 035067.
[49] X.H. Ruan, L. Pei, S.H. Xuan, Q.F. Yan, X.L. Gong, The rheological responds of the superparamagnetic fluid based on Fe_3O_4 hollow nanospheres, J. Magn. Magn. Mater. 429 (2017) 1–10.
[50] Q. Wen, A. Basu, P.A. Janmey, A.G. Yodh, Non-affine deformations in polymer hydrogels, Soft Matter 8 (31) (2012) 8039–8049.
[51] S.F. Medeiros, A.M. Santos, H. Fessi, A. Elaissari, Stimuli-responsive magnetic particles for biomedical applications, Int. J. Pharm. 403 (1-2) (2011) 139–161.
[52] S. Massou, F.N. Vicente, F. Wetzel, A. Mehidi, D. Strehle, C. Leduc, R. Voituriez, O. Rossier, P. Nassoy, G. Giannone, Cell stretching is amplified by active actin remodelling to deform and recruit proteins in mechanosensitive structures, Nat. Cell Biol. 22 (8) (2020) 1011 -+.
[53] D.S. Wong, J. Li, X. Yan, B. Wang, R. Li, L. Zhang, L. Bian, Magnetically tuning tether mobility of integrin ligand regulates adhesion, spreading, and differentiation of stem cells, Nano Lett. 17 (3) (2017) 1685–1695.
[54] S. Kakinoki, J.H. Seo, Y. Inoue, K. Ishihara, N. Yui, T. Yamaoka, Mobility of the Arg-Gly-Asp ligand on the outermost surface of biomaterials suppresses integrin-mediated mechanotransduction and subsequent cell functions, Acta Biomater. 13 (2015) 42–51.